Sensors and Actuators B 232 (2016) 43–51

Contents lists available at ScienceDirect

Sensors and Actuators B: Chemical

journal homepage: www.elsevier.com/locate/snb

Near-infrared absorption gas sensing with metal-organic framework on optical fibers

Xinyuan Chong[a], Ki-Joong Kim[b], Erwen Li[a], Yujing Zhang[b], Paul R. Ohodnicki[c,d], Chih-Hung Chang[b], Alan X. Wang[a,*]

[a] School of Electrical Engineering and Computer Science, Oregon State University, Corvallis, OR 97331, USA
[b] School of Chemical, Biological and Environmental Engineering, Oregon State University, Corvallis, OR 97331, USA
[c] National Energy Technology Lab, United States Department of Energy, Pittsburgh, PA 15236, USA
[d] Materials Science and Engineering Department, Carnegie Mellon University, Pittsburgh, PA 15213, USA

ARTICLE INFO

Article history:
Received 8 October 2015
Received in revised form 23 March 2016
Accepted 24 March 2016
Available online 25 March 2016

Keywords:
Infrared absorption
Fiber-optic sensors
Metal-organic
Framework
Gas sensors

ABSTRACT

Despite significant advantages in terms of portability and cost, near-infrared (NIR) gas sensing still remains a great challenge due to its relatively weak overtone absorption from the fundamental vibrational bond absorption at the mid-IR frequency. In this paper, we demonstrated ultra-sensitive NIR gas sensing for carbon dioxide (CO_2) at 1.57 μm wavelength through nanoporous Cu-BTC (BTC = benzene-1,3,5-tricarboxylate) metal-organic framework (MOF) coated single-mode optical fiber. For the first time, we obtained high-resolution NIR spectroscopy of CO_2 sorbed in MOF without seeing any rotational side band, indicating that the tightly confined gas molecules in the MOF pores do not have any freedom of rotation. Real-time measurement of the mixed gas flow of CO_2 and Ar showed different response time depending on the concentration of CO_2, which is attributed to the complex sorption mechanism of CO_2 in Cu-BTC MOF. Most importantly, we realized ultra-low detection limit of CO_2 (<20 ppm) with only 5 cm long Cu-BTC MOF thin film coated on single-mode optical fibers.

1. Introduction

Gas sensing plays pivotal roles in many applications including safety management of petrochemical industry [1], study of atmospheric science [2] and exhaust gas monitoring for combustion engines [3], to name a few. There are numerous gas sensing technologies available that allow trace-level detection of various gases [1,4–9]. Among them, optical sensors using infrared (IR) absorption spectroscopy [5,6,9,10] stands out due to the high detection specificity. IR spectroscopy relies on the optical absorption of molecular vibration bands, which represent the signatures of various gas molecules. Therefore, IR absorption spectroscopy is widely used as a simple and reliable technique for both detection and identification of hazardous and greenhouse gases. In addition, IR sensors have minimal drift, fast response, long lifetime, and can be conducted in real time and *in situ* without disturbing the target system.

The principle of infrared absorption gas sensing is based on Beer-Lambert law:

$$I = I_0 \exp(-\gamma \alpha L) \quad (1)$$

where I is the transmitted light intensity, I_0 is the incident intensity, α is the absorption coefficient of the analyte, which is determined by the gas concentration and is wavelength dependent. L is the absorption length which equals the actual interaction path between light and the gas sample, and γ is the enhancement factor determined by both the sensing media and the sensor structure. In free space system gas cells, $\gamma = 1$. While for evanescent field sensors, $\gamma < 1$ because of the partial overlap between the optical field and the gas analyte. According to the equation, there are two ways to increase the IR absorption: (1) to increase the interaction length L, for example, multi-path cavity is commonly used such as Herriott type gas cell [11]; (2) to increase the enhancement factor γ, for example, slow light effects from silicon photonic crystal waveguides has successfully enhanced the IR absorption by ~1000 times [12].

Both near-IR (NIR, 0.8–2.5 μm) and mid-IR (MIR, 2.5–25 μm) spectroscopies have been developed [13]. MIR spectroscopy offers remarkably high sensitivity by probing the fundamental vibrational and rotational transitions as the fingerprints of various gas

* Corresponding author.
E-mail address: wang@eecs.oregonstate.edu (A.X. Wang).

http://dx.doi.org/10.1016/j.snb.2016.03.135
0925-4005/

molecules. However, most commercial MIR spectroscopy systems such as Fourier transform-infrared spectroscopy (FT-IR) are large, expensive, and heavy tabletop instruments that consume relatively high power, which makes them unsuitable for mobile sensing applications. On the other hand, optical fiber communication systems for telecom industry have enabled NIR optoelectronic devices that are miniaturized, low cost, and highly reliable in the last few decades, which have significantly accelerated the progress of NIR gas sensors. The biggest challenge for NIR absorption spectroscopy sensors is that most gases do not have fundamental vibration bands at NIR regions. Instead, the absorptions have to come from the overtones of the fundamental vibration bands, hence it has relatively low detection sensitivity, and two or three orders of magnitude lower than that of the MIR sensing.

In recent years, metal-organic frameworks (MOFs) consisting of metal ions or ion clusters and bridging organic ligands have drawn great research interests as a new class of nanoporous material for gas storage [14–17], chemical separation [18–20], catalysis [21–23], molecular recognition [24–26], drug delivery [27–29] and sensor [4,10,30–33]. Cu-BTC (BTC = benzene-1,3,5-tricarboxylic acid) [34], one of the earliest reported MOFs, has been extensively investigated both theoretically and experimentally. Due to its easy synthesis and large porosity, it has been widely applied to gas storage.

Previously, we developed an ultra-short NIR fiber-optic CO_2 sensor through Cu-BTC MOF thin films [10] to enhance the intrinsically low sensitivity of NIR spectroscopy. The proof-of-concept has been demonstrated by an 8-cm long multimode fiber (MMF) sensor coated with 100 nm thick Cu-BTC MOF thin film. However, many fundamental issues related to the sensing mechanism of CO_2 in MOF have not been revealed, and the detection limit of 500 ppm is still above the CO_2 concentration in the ambient atmosphere. In this paper, we prepared Cu-BTC MOF thin films on standard single-mode fibers (SMFs) to enhance the sensitivity. For the first time, we obtained high-resolution NIR spectroscopy of CO_2 sorbed in MOF without seeing any rotational side band, suggesting that the bound or tightly confined gas molecules in the pores of Cu-BTC MOF do not have any freedom of rotation. We also conducted real-time measurement to obtain the sensing time of different CO_2 concentrations, which is correlated to the complex sorption mechanism of CO_2 in Cu-BTC pores. Last but not least, we obtained ultra-low detection limit of CO_2 down to 20 ppm with only 5 cm long Cu-BTC MOF thin films on single-mode fibers.

2. Experimental

2.1. Materials

Copper acetate ($Cu(OAc)_2$, 98%), copper nitrate hexahydrate ($Cu(NO_3)_2{\cdot}6H_2O$, 99%) and benzene-1,3,5-tricarboxylic acid (BTC, 95%) were purchased from Sigma-Aldrich. American Chemical Society (ACS) grade of ethanol (>99.5%) from Macron chemicals was used as the solvent. All chemicals were used as purchased without further purification. The optical fibers purchased from Thorlabs, Inc. were standard SMF-28 for optical telecommunication network.

2.2. Sensor fabrication

The fiber-optic sensor was fabricated by growing nanoporous Cu-BTC MOF on the surface of the core of a SMF. Briefly, a 1 m long SMF was fixed on a silicon substrate by UV epoxy after removing the polymer coating layer by flame. Standard buffered oxide etchant (BOE) was then used to etch away the cladding layer of the SMF by merging the silicon substrate into the BOE solution. During the etching process, the fiber was connected to a 1.55 μm laser diode and an optical power meter was used to monitor the optical transmission through the SMF. When the transmitted optical power dropped 1.5–2 dB, the etching process was stopped by taking out the silicon substrate from the BOE and rinsing with deionized water. The length of the etched region of the SMF was 5-cm long.

MOFs were grown on both the surface of etched region of SMF and a piece of sapphire substrate by layer-by-layer (LBL) method [35]. The SMF was first treated by oxygen plasma and then immersed in a 300 mL ethanol solution which contains 10 mM metal precursor $Cu(OAc)_2$ for 20 min. Subsequently, the SMF was immersed in another 300 mL ethanol solution which contains 1 mM organic ligand BTC for 40 min. Between each step, the fiber was rinsed with ethanol to remove the unreacted precursor ions or molecules to ensure the uniform growth and then naturally dried at room temperature (295.5 K) for 10 min. Cu-BTC MOF thin film on SMF was grown by 40 cycles LBL method.

For comparison, bulk Cu-BTC synthesized *via* a typical solvothermal method in a batch reactor was also prepared. A solution of $Cu(NO_3)_2$ (3.6 mM) in 60 mL of ethanol and BTC (8.1 mmol) in 60 mL of ethanol were both stirred for 10 min in a 250 mL beaker, separately. A 50/50 mixture of $Cu(NO_3)_2$ and BTC solution was stirred for 10 min, then was placed in a Teflon autoclave. The sealed autoclave was heated to 120 °C, held for 18 h in a convective oven, and cooled to room temperature naturally. The collected reaction products were washed with ethanol 3 times and were dried under vacuum for 24 h at 70 °C. Nitrogen sorption/desorption isotherm was measured at −196 °C with a Micromeritics ASAP 2010 analyzer. The samples were degassed in vacuum for 2 h at 150 °C prior to analysis. The Brunauer-Emmett-Teller (BET) surface areas were obtained from the amount of N_2 physisorbed at different relative pressures (P/P_0), based on the linear part of the 6 point sorption data at $P/P_0 = 0.02–0.10$. The total pore volume was calculated by the Horvath Kawazoe method at $P/P_0 = 0.99$. The mesopore volume and micropore volume were obtained by the Barrett-Joyner-Halenda sorption and the *t*-plot methods, respectively. The pore size distribution was evaluated by the original density functional theory model. Scanning electron microscope (SEM) analysis was conducted with an FEI Quanta 600 using 5–10 kV accelerating voltage.

2.3. Experimental setup

The experimental setup for CO_2 sensing is shown in Fig. 1. A tunable semiconductor laser diode (HP 8168) and an amplified spontaneous emission (ASE) light source (Thorlabs, Inc. S5FC1550S-A2) were used to couple light into the fiber-optic sensor by fusion splicing another SMF with the gas sensor. Fusion splicing improved the coupling stability by 20 dB compared with optical coupling using 3-axis stages and therefore enhanced the signal-to-noise ratio (SNR). The gas sensor was placed inside a gas cell, which was connected to CO_2 and Ar gases. The transmitted light through the sensor was directly coupled to a power meter (Thorlabs, Inc. S122C) or an optical spectrum analyzer (Thorlabs, Inc. OSA203), and the data were collected by a personal computer. Flow rates of gas were controlled by mass flow controllers (MFC) (Aalborg, GFC 17) with 0–20 mL min^{-1} flow range. Different CO_2 concentration was achieved by varying the mixing ratio of CO_2 and Ar flows.

3. Results and discussion

3.1. Characterization

SEM images of the MOF-coated fiber optic sensor are shown in Fig. 2 (a)–(c), which clearly shows that the Cu-BTC MOF crystals covered the entire surface of the etched region. The discrete MOF crystals results in a rough surface. In addition, we did not observe

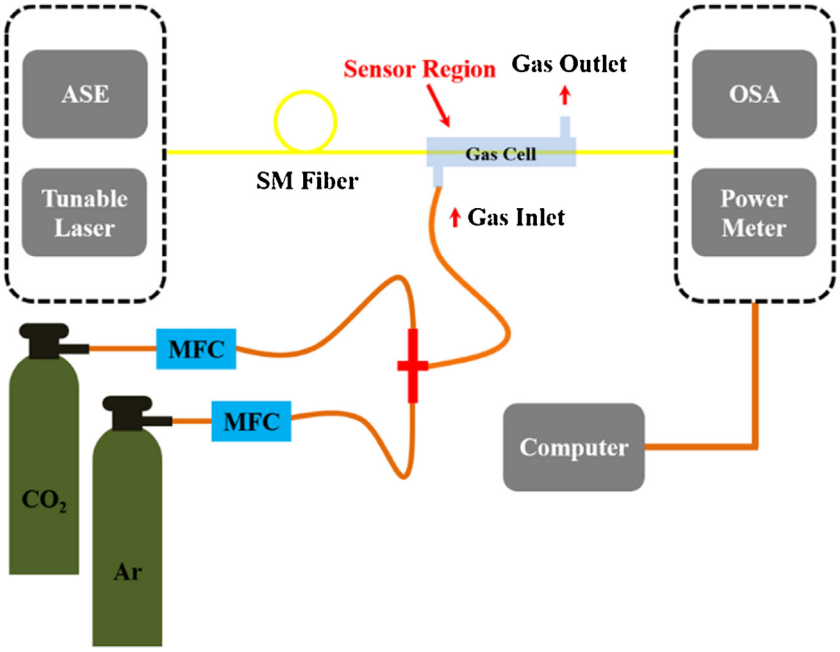

Fig. 1. Schematic of the experimental setup for CO_2 sensing used in this study. ASE: Amplified spontaneous emission; OSA: Optical spectrum analyzer; MFC: Mass flow controller.

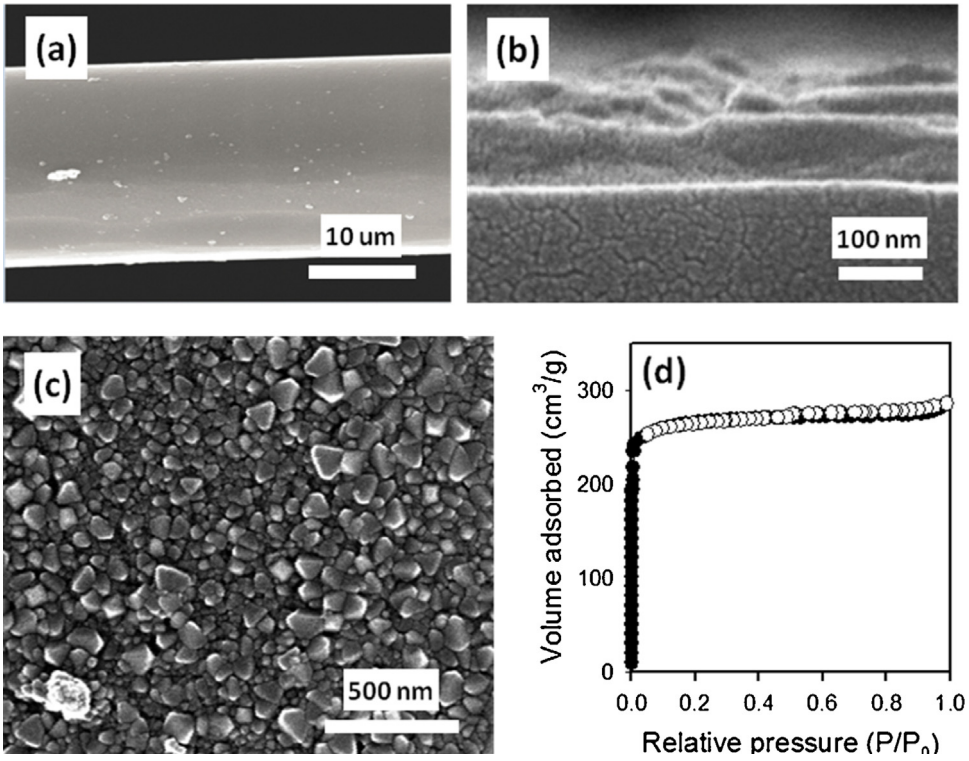

Fig. 2. (a) Low resolution and high resolution (b) cross section and (c) top SEM images of MOF-coated SMF by LBL method. (d) N_2 gas isotherm of the bulk Cu-BTC MOF.

any peel-off of MOF crystals from the SMF, indicating good bonding between the surface of fiber optic and MOF. Cross-sectional SEM image in Fig. 2(b) shows a dense and uniform film with thickness of 100 nm. In our previous results, Cu-BTC MOF thin film on the surface of MMFs shows the oriented growth with (111) direction, indicating well developed crystal structure of Cu-BTC [10]. The total volume and surface area of Cu-BTC thin film on the surface of single-mode fibers were estimated form the texture properties of the bulk Cu-BTC MOF synthesized by solvothermal method, because it is very difficult to measure the sorbed amount of gas on MOF thin films. Fig. 2(d) shows the N_2 gas sorption-desorption isotherm of the bulk Cu-BTC MOF. Isotherm shows a typical characteristic of microporous materials rapidly increased at a lower P/P_0, with a small hysteresis loop associated with capillary condensation in the mesoporous structures, most probably from intra agglomerate voids in the particle. Physical properties of Cu-BTC MOF bulk and

Table 1
Texture properties of the Cu-BTC MOF bulk and thin film.

Cu-BTC bulk				Cu-BTC film			
S_{BET}(m^2 g^{-1})[a]	Pore volume (cm^3 g^{-1})			Thickness(nm)	Length(cm)	Volume[e](um^3)	Surface area(m^2)[f]
	V_{total}[b]	V_{meso}[c]	V_{micro}[d]				
886	0.441	0.078	0.364	100	5	3×106	0.93×10^{-3}

[a] BET surface area.
[b] Total pore volume.
[c] Mesopore volume.
[d] Micropore volume.
[e] Total volume of MOF film on fiber.
[f] Estimated from S_{BET} of bulk Cu-BTC.

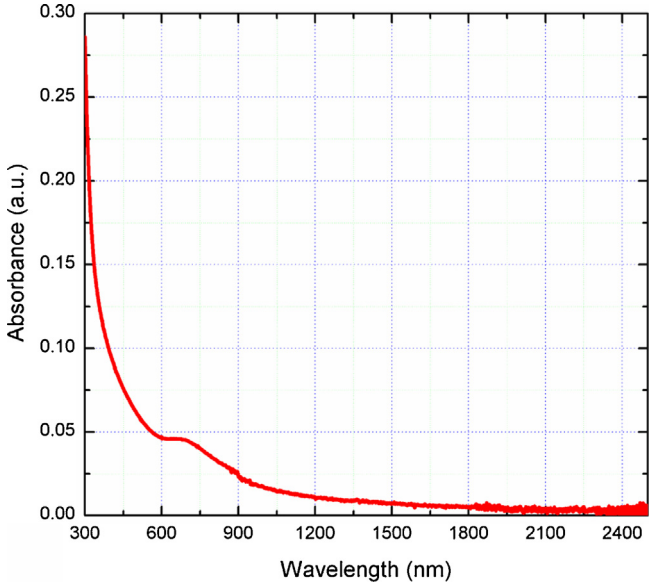

Fig. 3. Absorbance spectrum of 100 nm thick Cu-BTC MOF coated on sapphire substrate.

thin film are summarized in Table 1. The estimated surface area of the Cu-BTC thin film on the surface of SMF fabricated in this work was 0.93×10^{-3} m^2.

Optical properties of MOF thin films were studied by UV–vis-NIR spectrometer. The absorbance spectrum of 100 nm thick Cu-BTC MOF film grown on 300 μm sapphire substrate was measured, and the result is shown in Fig. 3. One absorption peak was observed around 700 nm, which is attributed to the d-d band absorption of typical copper carboxylate complexes in the crystal structure of Cu-BTC MOF. At CO_2 absorption band (1565–1585 nm), the absorption is very close to zero. Due to the approach that UV–vis-NIR spectrometer measuring the absorbance, Fig. 3 actually represents both absorption and scattering. Considering the highly rough surface of MOF layer, the small portion of "Absorbance" that is monitically decreasing with wavelength is acutally the scattering.

3.2. Absorption spectrum of CO_2

ASE light source and OSA were used to obtain the absorption spectrum for the MOF-coated SMF sensor. Prior to the measurement, the sensor was purged with pure Ar gas for 12 h to remove all the gas molecues, especially the water vapor inside the porous structures. After that, the transmission spectrum was collected as the reference. Then, the gas flow was switched from pure Ar to pure CO_2. The transmission spectrum was collected when it became stable. The absorption spectrum was calculated based on Beer-Lambert law and is shown in Fig. 4(a). As a comparison, the absorption spectrum of gas phase CO_2 in a 10 cm quartz gas cell (PIKE Technologies Inc. 162-1810) was also measured, as shown in Fig. 4(b). For gas phase CO_2, it exhibited both vibrational bands and rotational fine lines which matched with the theoretical results from HITRAN database. However, for CO_2 sorbed MOF film, unlike the gas phase CO_2, a broad absorption peak between 1568–1572 nm was observed. The missing rotational fine lines of the absorption spectrum was attributed to energy transition change of the rotational states caused by the bonding effect of the gas molecules inside the MOF pores. The discrepancy of the peak position of these two spectra can also possibly be caused by the interaction between CO_2 molecules and sorption sites in MOF [36]. Besides, the multiple peaks between 1576 nm and 1588 nm should be the other vibrational band at 1576–1583 nm, since these peaks are repeatable in the experiments. However we still do not fully understand why the absorption peak splits into multiple peaks and why these absorption peaks are weaker than the one at 1568–1572 nm. It is possible that the bonding state also changed the symmetry of the vibrational bands. Further quantitative investigation will be conducted in the future work.

3.3. Dynamic response

To investigate the dynamic response of the sensor, the light source and detector were changed to a tunable laser diode and a power meter. The wavelength of the tunable laser was fixed at 1569 nm, which is the absorption peak of CO_2 in MOF as shown in Fig. 4(b). The real-time response was studied by monitoring the transmission power when switching pure Ar and CO_2 flows alternatively. As shown in Fig. 5(a), the response time for low and high concentration CO_2 are significantly different. At low concentration, both sorption and desorption time are much longer than that of at high concentration CO_2. Fig. 5(b) and (d) shows the optical transmittance of CO_2 during sorption and desorption processes with 100% CO_2 and 100% Ar flowing. It can be seen that at high concentration, the sorption (from 90% to 10%) and desorption time (from 10% to 90%) are 10 s and 12 s, respectively. However, at low concentration (30 ppm CO_2 in Ar), both processes become much slower as shown in Fig. 5(c) and (e).

This significant difference can be explained by different sorption and desorption kinetics at high and low CO_2 concentration [37–39]. At high concentration, most of the gas molecules are physically sorbed inside the MOF pores. Due to the relatively small activation barrier of physisorption, the sorption and desorption rate can be very fast, which is determined by the concentration gradient. Moreover, the process is reversible, as shown in Fig. 5(b) and (d). On the other hand, at low concentration CO_2, chemical bonding becomes dominant instead of physical bonding. This chemisorption behavior inside Cu-BTC pore is expected to be complicated, since there are three sorption sites exhibiting different interaction energy: (1) unsaturated metal site (UM), (2) tetrahedral cage opening site (TCO) and (3) center of tetrahedral cage site (CTC) [40]. The most stable site is the UM site (sorp-

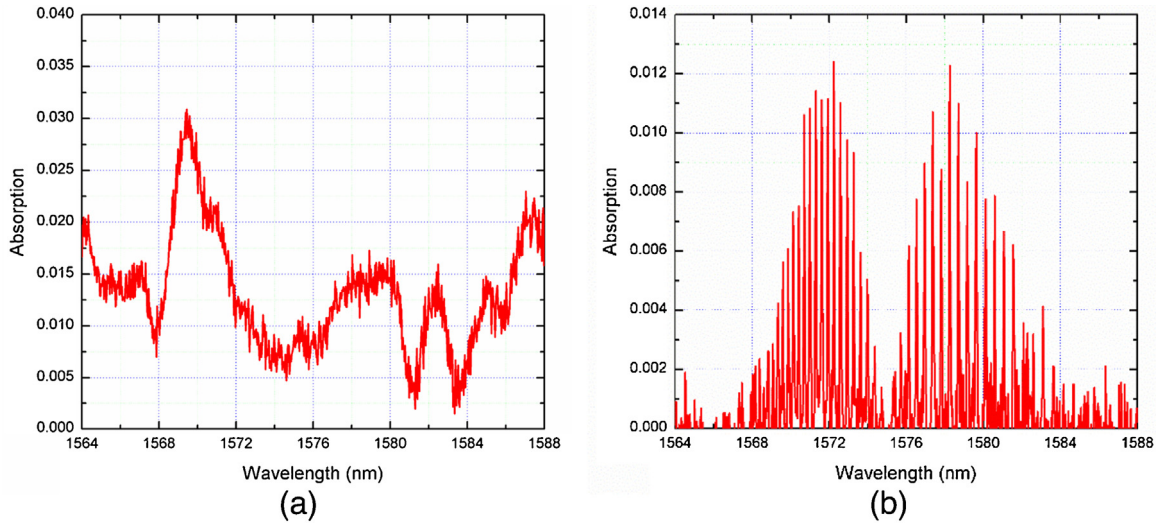

Fig. 4. Absorption spectra of (a) CO_2 bound inside MOF and (b) gas phase CO_2 inside quartz gas cell.

tion energy: $-28.2\,kJ\,mol^{-1}$), where CO_2 molecules interact with Cu^{2+}. The TCO and CTC are less stable than UM sites, whose interaction energies are almost the same, about $5\,kJ\,mol^{-1}$ less stable than UM sites. When CO_2 is flowed, CO_2 molecules are preferentially first sorbed on the twelve UM sites in a unit cell. Only after all the UM sites are occupied (CO_2:Cu^{2+} ratio >12:12), TCO sites will start to sorb gas molecules. When the CO_2:Cu^{2+} ratio is greater than 20:12, CTC sites will start to sorb gas molecules. If the concentration is even higher, the large pores will also start to sorb CO_2 molecules in the pores. Although bonding energy will not act as an activation barrier, the sorption activation barrier for chemical bonding is still higher than physical bonding, which will lead to a longer response time. For the desorption process, since certain amount of energy is required to break the chemical bonding and release the CO_2 molecules, therefore longer response time are needed.

3.4. Effect of nitrogen and water vapor

For real gas sensing, the interference from other gases such as nitrogen (N_2) and water vapor cannot be ignored. In this paper, the effect of these two most significance gases was also studied. The experiments are conducted under room temperature (295.5 K). For N_2, the purging gas was changed from Ar to N_2, and the response of the sensor for pure (100%) CO_2 is shown in Fig. 6(a). Compared to Ar, the response time of N_2 purging became much longer. Unlike Ar which is not sorbed by MOF at all, N_2 can still be sorbed in MOF pores, although the sorbing affinity is lower than CO_2. Therefore, after purging with N_2, some of the pores in MOF will remain occupied. When changing the flow gas to CO_2, the CO_2 gas molecules have to repel the N_2 molecules in the pores, which results in a much longer response time. For real engineering applications, neither Ar nor N_2 purging are efficient methods. To quickly reset the SMF gas sensor, heating and/or vacuum are anticipated to be a better way to release the sorbed CO_2 from the MOF pores.

Water vapor is another major interference since the sorption affinity to MOF is much higher than CO_2. Especially for Cu-BTC, which is hydrophilic, both theoretical and experimental investigations have shown a strong affinity of water molecules [41,42]. The effect of water vapor is qualitatively studied using a simple setup shown in Fig. 6(b). Briefly, pure (100%) CO_2 gas passes through a water bath before entering the gas cell. If the innet gas tube is immersed below the water surface, water vapor close to the saturation pressure at room temperature will be mixed with CO_2. If the innet gas tube is placed above the water surface, water vapor pressure in the mixed gas will be less than the saturation pressure. The spectral response of the sensor is shown in Fig. 6(c). It is seen that adding water vapor into the CO_2 flow will drastically alter the sensor response. Due to the competitive sorption between CO_2 and water vapor, more water vapor is taken by MOF and occupies most of the sorption sites. Therefore, the amount of CO_2 molecules that can be sorbed by MOF is signficantly reduced. In addition, the NIR absorption coefficient of water vapor at 1.57 μm is about two orders of magnitude lower than that of CO_2 according to HITRAN database. As a result, the CO_2 absorption band becomes less observable and the overall NIR absorption is reduced as the water vapor in the CO_2 flow increases. Based on our experimental work, an desiccation process is neccessary to remove the water vapor. Actually, many gas sensors suffer the interference from water vapor when working in real environment [43]. In order to eliminate the effect of water vapor, several methods have been developed, such as silica gel desiccant dryer [44], thermoelectric cooler [45] and vapor separation membrane [46–48]. Among them, the Nafion membrane has the best performance and is widely used for water vapor separation. Therefore, for the future practical application, a Nafion membrane can be used to wrap around the gas sensor to remove the water vapor, which is very straightforward.

3.5. Detection limit

The detection limit was studied by measuring the change of the transmission power as a function of CO_2 concentration. Different CO_2 concentration was controlled by diluting with Ar. As shown in Fig. 7(a), the lowest concentration that can be detected was about 20 ppm, which is one order lower as compared with the previously reported MOF-coated MMF sensor [10]. The enhancement factor γ was calculated based on the Beer-Lambert law, as shown in Fig. 7(b). The γ is not a linear function of CO_2 concentration, and is larger at lower concentration. Usually, the evanescent field optical sensors have lower γ (<1) due to the weaker light-matter interaction. However, MOF can concentrate CO_2 inside the poros resulting in a much higher CO_2 molecule than the ambient evironment. Therefore, the actual γ (>1) is the combined result of evansecent field and CO_2 concentration effect in MOF pores.

Here we define the figure-of-merit (*FOM*) = sensitivity × optical pathlength. Therefore, the *FOM* of our gas sensor is 100 ppm cm. Sonnenfroh et al. [49] reported CO_2 sensor with 0.09 ppm sensitivity using a 20 cm integrated cavity at 2.0 μm wavelength.

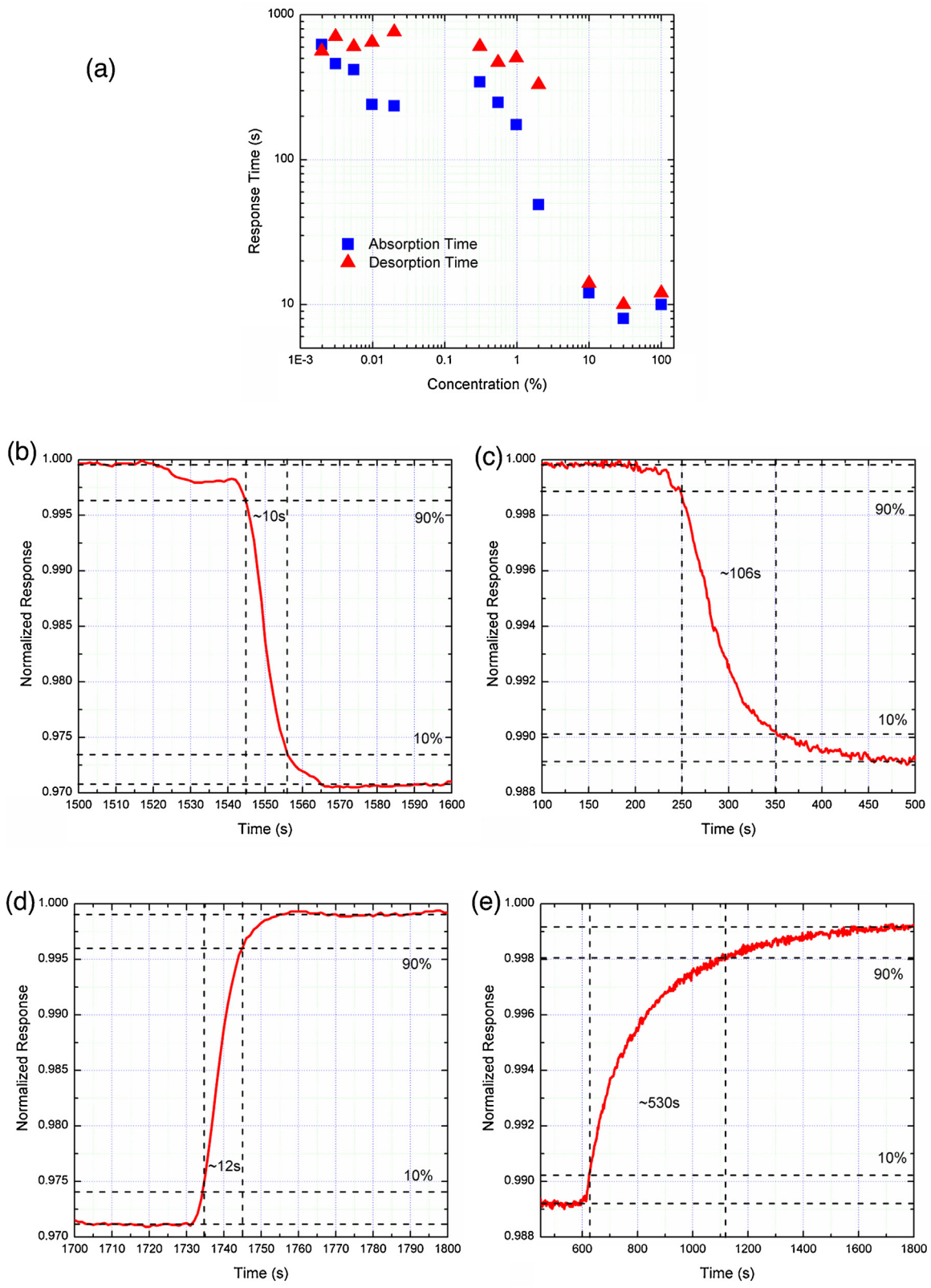

Fig. 5. Dynamic responses of the MOF-coated SMF sensor for alternating pure Ar and CO_2–containing flows: (a) sorption time and desorption time as a function of CO_2 concentration; (b,c) sorption time and (d,e) desorption time for pure CO_2 and 30 ppm CO_2, respectively.

However, the actual optical length reaches ~50 m which results in *FOM* = 450 ppm cm. Besides, the absorption coefficient at 2.0 μm is about 70 times higher than that of at 1.57 μm. Hawe et al. [50] used an integrating sphere to achieve 200 ppm sensitivity. The optical length is 114 cm which gives $FOM = 2.28 \times 10^4$ ppm cm. Compared with these recently reported NIR CO_2 sensors, our sensor shows the best *FOM*. Table 2 lists the key parameters of the sensor.

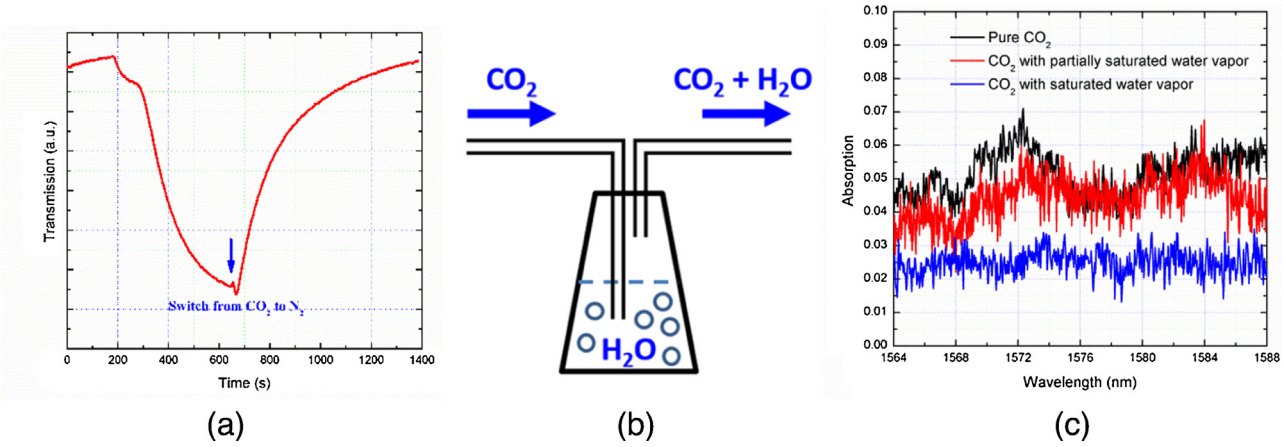

Fig. 6. (a) Response time of the SMF sensor when purged by pure N_2 and CO_2. (b) Setup for mixing water vapor with CO_2. (c) The absorption spectra of CO_2 with and without vapor.

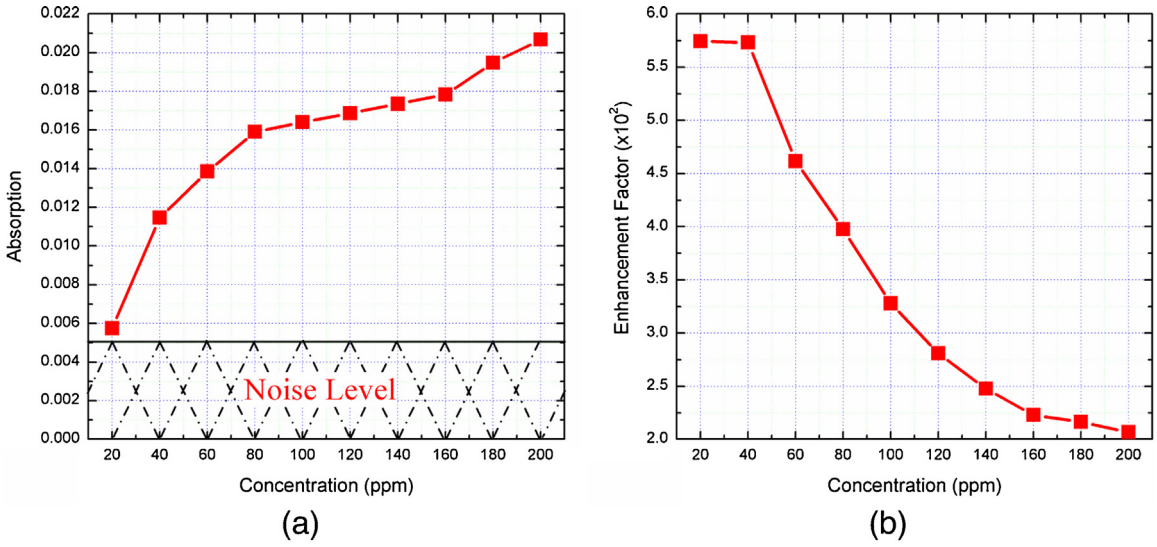

Fig. 7. (a) Average absorption and (b) enhancement factor as a function of CO_2 volume concentration in Ar.

Table 2
Key parameters of the sensor.

Detection Limit (ppm)	FOM (ppm cm)	Noise Level (μW)[a]	Response Time (s)	Sensor Length (cm)
20	100	~0.2	8–625/10–710	5

[a] Above the noise level, the power change of the transmission light due to the absorption can be detected.

4. Conclusion

In summary, we demonstrate ultra-sensitive NIR sensing of CO_2 at 1.57 μm with MOF coated on SMFs. We obtain high-resolution NIR spectroscopy of CO_2 sorbed in MOF, which indicates an interesting phenomenon that the tightly confinement gas molecules inside MOF do not show rotation side bands as they are in free space. Real-time measurement of the sorption and desorption time at low and high concentration of CO_2 further reveals the complex sorption mechanism of CO_2 in Cu-BTC MOF. Moreover, the detection limit is improved down to 20 ppm with only 5 cm sensing region. The *FOM* is demonstrated to be 100 ppm cm, which is the best compared with recent reported NIR CO_2 sensors.

Acknowledgements

This technical effort was performed in support of the National Energy Technology Laboratory's (NETL) research under the RES contract DE-FE0004000 and the National Science Foundation under grant No. 1449383. Xinyuan Chong and Yujing Zhang are sponsored by the Graduate Student Fellowship from NETL.

References

[1] D.E. Vogler, M.W. Sigrist, Near-infrared laser based cavity ringdown spectroscopy for applications in petrochemical industry, Appl. Phys. B-Lasers Opt. 85 (2006) 349–354.
[2] V. Ramanathan, Y. Feng, Air pollution, greenhouse gases and climate change: global and regional perspectives, Atmos. Environ. 43 (2009) 37–50.
[3] N. Docquier, S. Candel, Combustion control and sensors: a review, Prog. Energy Combust. 28 (2002) 107–150.

[4] K.J. Kim, X.Y. Chong, P.B. Kreider, G.H. Ma, P.R. Ohodnicki, J.P. Baltrus, et al., Plasmonics-enhanced metal-organic framework nanoporous films for highly sensitive near-infrared absorption, J. Mater. Chem. C 3 (2015) 2763–2767.
[5] W.C. Lai, S. Chakravarty, X.L. Wang, C.Y. Lin, R.T. Chen, On-chip methane sensing by near-IR absorption signatures in a photonic crystal slot waveguide, Opt. Lett. 36 (2011) 984–986.
[6] N. Gayraud, L.W. Kornaszewski, J.M. Stone, J.C. Knight, D.T. Reid, D.P. Hand, et al., Mid-infrared gas sensing using a photonic bandgap fiber, Appl. Opt. 47 (2008) 1269–1277.
[7] O. Frazao, J.L. Santos, F.M. Araujo, L.A. Ferreira, Optical sensing with photonic crystal fibers, Laser Photonics Rev. 2 (2008) 449–459.
[8] M.H. Chiu, S.F. Wang, R.S. Chang, D-type fiber biosensor based on surface-plasmon resonance technology and heterodyne interferometry, Opt. Lett. 30 (2005) 233–235.
[9] Y.L. Hoo, W. Jin, H.L. Ho, D.N. Wang, R.S. Windeler, Evanescent-wave gas sensing using microstructure fiber, Opt. Eng. 41 (2002) 8–9.
[10] X. Chong, K. Kim, P. Ohodnicki, E. Li, C. Chang, A. Wang, Ultra-short near-infrared fiber-optic sensors for carbon dioxide detection, Sens. J. IEEE (2015) 5327–5332.
[11] D. Herriott, H. Kogelnik, R. Kompfner, Off-axis paths in spherical mirror interferometers, Appl. Opt. 3 (1964) 523–526.
[12] W.C. Lai, S. Chakravarty, X.L. Wang, C.Y. Lin, R.T. Chen, Photonic crystal slot waveguide absorption spectrometer for on-chip near-infrared spectroscopy of xylene in water, Appl. Phys. Lett. 98 (2011).
[13] J.J.R. Rohwedder, C. Pasquini, P.R. Fortes, I.M. Raimundo, A. Wilk, B. Mizaikoff, iHWG-[small mu]NIR: a miniaturised near-infrared gas sensor based on substrate-integrated hollow waveguides coupled to a micro-NIR-spectrophotometer, Analyst 139 (2014) 3572–3576.
[14] K. Sumida, D.L. Rogow, J.A. Mason, T.M. McDonald, E.D. Bloch, Z.R. Herm, et al., Carbon dioxide capture in metal-organic frameworks, Chem. Rev. 112 (2012) 724–781.
[15] Y.S. Bae, R.Q. Snurr, Development and evaluation of porous materials for carbon dioxide separation and capture, Angew. Chem. Int. Ed. 50 (2011) 11586–11596.
[16] N.L. Rosi, J. Eckert, M. Eddaoudi, D.T. Vodak, J. Kim, M. O'Keeffe, et al., Hydrogen storage in microporous metal-organic frameworks, Science 300 (2003) 1127–1129.
[17] M. Dinca, J.R. Long, Hydrogen storage in microporous metal-organic frameworks with exposed metal sites, Angew. Chem. Int. Ed. 47 (2008) 6766–6779.
[18] J.R. Li, J. Sculley, H.C. Zhou, Metal-organic frameworks for separations, Chem. Rev. 112 (2012) 869–932.
[19] J.S. Seo, D. Whang, H. Lee, S.I. Jun, J. Oh, Y.J. Jeon, et al., A homochiral metal-organic porous material for enantioselective separation and catalysis, Nature 404 (2000) 982–986.
[20] S.C. Xiang, Z.J. Zhang, C.G. Zhao, K.L. Hong, X.B. Zhao, D.R. Ding, et al., Rationally tuned micropores within enantiopure metal-organic frameworks for highly selective separation of acetylene and ethylene, Nat. Commun. 2 (2011).
[21] J. Lee, O.K. Farha, J. Roberts, K.A. Scheidt, S.T. Nguyen, J.T. Hupp, Metal-organic framework materials as catalysts, Chem. Soc. Rev. 38 (2009) 1450–1459.
[22] M. Yoon, R. Srirambalaji, K. Kim, Homochiral metal-organic frameworks for asymmetric heterogeneous catalysis, Chem. Rev. 112 (2012) 1196–1231.
[23] D.B. Dang, P.Y. Wu, C. He, Z. Xie, C.Y. Duan, Homochiral metal-organic frameworks for heterogeneous asymmetric catalysis, J. Am. Chem. Soc. 132 (2010) 14321–14323.
[24] T. Uemura, N. Yanai, S. Kitagawa, Polymerization reactions in porous coordination polymers, Chem. Soc. Rev. 38 (2009) 1228–1236.
[25] M. Albrecht, M. Lutz, A.L. Spek, G. van Koten, Organoplatinum crystals for gas-triggered switches, Nature 406 (2000) 970–974.
[26] B.L. Chen, Y. Yang, F. Zapata, G.N. Lin, G.D. Qian, E.B. Lobkovsky, Luminescent open metal sites within a metal-organic framework for sensing small molecules, Adv. Mater. 19 (2007) 1693.
[27] P. Horcajada, T. Chalati, C. Serre, B. Gillet, C. Sebrie, T. Baati, et al., Porous metal-organic-framework nanoscale carriers as a potential platform for drug delivery and imaging, Nat. Mater. 9 (2010) 172–178.
[28] P. Horcajada, C. Serre, G. Maurin, N.A. Ramsahye, F. Balas, M. Vallet-Regi, et al., Flexible porous metal-organic frameworks for a controlled drug delivery, J. Am. Chem. Soc. 130 (2008) 6774–6780.
[29] J. Della Rocca, D.M. Liu, W.B. Lin, Nanoscale metal-organic frameworks for biomedical imaging and drug delivery, Acc. Chem. Res. 44 (2011) 957–968.
[30] L.E. Kreno, K. Leong, O.K. Farha, M. Allendorf, R.P. Van Duyne, J.T. Hupp, Metal-organic framework materials as chemical sensors, Chem. Rev. 112 (2012) 1105–1125.
[31] T.H. Yu, C.H. Ho, C.Y. Wu, C.H. Chien, C.H. Lin, S. Lee, Metal-organic frameworks: a novel SERS substrate, J. Raman Spectrosc. 44 (2013) 1506–1511.
[32] Y.L. Hu, J. Liao, D.M. Wang, G.K. Li, Fabrication of gold nanoparticle-embedded metal-organic framework for highly sensitive surface-enhanced raman scattering detection, Anal. Chem. 86 (2014) 3955–3963.
[33] R.J.T. Houk, B.W. Jacobs, F. El Gabaly, N.N. Chang, A.A. Talin, D.D. Graham, et al., Silver cluster formation, dynamics, and chemistry in metal-organic frameworks, Nano Lett. 9 (2009) 3413–3418.
[34] S.S.Y. Chui, S.M.F. Lo, J.P.H. Charmant, A.G. Orpen, I.D. Williams, A chemically functionalizable nanoporous material [Cu-3(TMA)(2)(H2O)(3)](n), Science 283 (1999) 1148–1150.
[35] O. Shekhah, H. Wang, S. Kowarik, F. Schreiber, M. Paulus, M. Tolan, et al., Step-by-step route for the synthesis of metal-organic frameworks, J. Am. Chem. Soc. 129 (2007) 15118.
[36] J.M. Schloss, Infrared Spectroscopy of Trapped Gases in Metal-Organic Frameworks. Honors Theses, Oberlin College, 2011.
[37] M. Thommes, K. Kaneko, A.V. Neimark, J.P. Olivier, F. Rodriguez-Reinoso, J. Rouquerol, et al., Physisorption of gases, with special reference to the evaluation of surface area and pore size distribution (IUPAC Technical Report), Pure Appl. Chem. 87 (2015) 1051–1069.
[38] F.R.J. Rouquerol, K.S.W. Sing, P. Llewellyn, G. Maurin, Adsorption by Powders and Porous Solids: Principles Methodology and Applications, Academic Press, 2014.
[39] J. Garrido, A. Linaressolano, J.M. Martinmartinez, M. Molinasabio, F. Rodriguezreinoso, R. Torregrosa, Use of N2 Vs Co2 in the characterization of activated carbons, Langmuir 3 (1987) 76–81.
[40] L. Grajciar, A.D. Wiersum, P.L. Llewellyn, J.S. Chang, P. Nachtigall, Understanding CO2 adsorption in CuBTC MOF: comparing combined DFT-ab initio calculations with microcalorimetry experiments, J. Phys. Chem. C 115 (2011) 17925–17933.
[41] J.J. Gutierrez-Sevillano, S. Calero, R. Krishna, Selective adsorption of water from mixtures with 1-alcohols by exploitation of molecular packing effects in CuBTC, J. Phys. Chem. C 119 (2015) 3658–3666.
[42] F. Gul-E-Noor, B. Jee, A. Poppl, M. Hartmann, D. Himsl, M. Bertmer, Effects of varying water adsorption on a Cu-3(BTC)(2) metal-organic framework (MOF) as studied by H-1 and C-13 solid-state NMR spectroscopy, Phys. Chem. Chem. Phys. 13 (2011) 7783–7788.
[43] G. Korotcenkov, Chemical Sensors: Simulation and Modeling Volume 2: Conductometric-Type Sensors, Momentum Press, 2012.
[44] P. Gandhidasan, A.A. Al-Farayedhi, A.A. Al-Mubarak, Dehydration of natural gas using solid desiccants, Energy 26 (2001) 855–868.
[45] C. Yildirim, S.K. Soylu, I. Atmaca, I. Solmus, Experimental investigation of a portable desalination unit configured by a thermoelectric cooler, Energy Convers. Manag. 85 (2014) 140–145.
[46] J.S. Cha, R. Li, K.K. Sirkar, Removal of water vapor and VOCs from nitrogen in a hydrophilic hollow fiber gel membrane permeator, J. Membr. Sci. 119 (1996) 139–153.
[47] S.J. Metz, W.J.C. van de Ven, J. Potreck, M.H.V. Mulder, M. Wessling, Transport of water vapor and inert gas mixtures through highly selective and highly permeable polymer membranes, J. Membr. Sci. 251 (2005) 29–41.
[48] K.J. Leckrone, J.M. Hayes, Efficiency and temperature dependence of water removal by membrane dryers, Anal. Chem. 69 (1997) 911–918.
[49] D. Sonnenfroh, K. Parameswaran, Diode laser-based sensor for high precision measurements of ambient CO2 in network applications, Appl. Phys. B-Lasers Opt. 102 (2011) 407–416.
[50] E. Hawe, P. Chambers, C. Fitzpatrick, E. Lewis, CO2 monitoring and detection using an integrating sphere as a multipass absorption cell, Meas. Sci. Technol. 18 (2007) 3187–3194.

Biographies

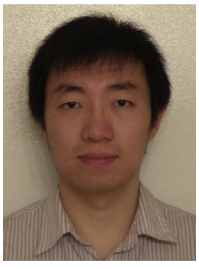

Xinyuan Chong is a Ph.D. candidate of the School of Electrical Engineering and Computer Science at Oregon State University. He received his B.S. and M.S. in Physics from Tsinghua University in 2008 and 2011 respectively. His current research interests include plasmonic-enhanced optical sensor for chemical detection, gas sensing, and biomedical applications.

Dr. Ki-Joong Kim received his Ph.D. degree in Chemical Engineering from Sunchon National University, South Korea in 2009. During his Ph.D work, he focused on the synthesis and characterization of nanomaterials for environmental processes such as adsorption processes and catalytic reactions using modified activated carbons, zeolites, and nanocatalysts. Dr. Ki-Joong Kim currently is a postdoctoral researcher at Oregon State University. His main work has been focused on synthesis of functional materials such as nanocrystals, quantum dots, and metal-organic frameworks with ultra-high surface area, and use them for energy and environmental applications, including photovoltaics, gas storage/separations, hydrogen storage, catalysts, luminescence, and gas sensing.

Erwen Li is a Ph.D. candidate of the School of Electrical Engineering and Computer Science at Oregon University. He received his B.S. in Physics from Fudan University in 2011. His current research interests include nanostructured photonic devices for sensing and spectroscopic application.

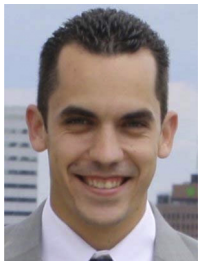

Dr. Paul Ohodnicki is a staff scientist and the Team Leader of the Electrochemical and Magnetic Materials Team within the Functional Materials Development Division of the National Energy TechnologyLaboratory (NETL). He is responsible for overseeing several major projects in the areas of functional sensor materials for power generation and sub-surface applications including solid oxide fuel cells and unconventional resource recovery such as shale gas as advanced anode and cathode engineering in solid oxide fuel cells through infiltration. His primary research interests are focused on studies of nanostructured and nanocomposite material systems with a particular emphasis on materials for sensors, power electronics, and energy conversion devices. Prior to his current role at the NETL, Paul was a staff scientist in the Chemistry and Surface Science Division from 2011 to 2013 and he also worked in a program management role for the Solid State Energy Conversion Alliance (SECA) program in 2010 focused on development and deployment of large scale solid oxide fuel cell technology. Paul also spent several years as a Research and Development Engineer at PPG Industries where he worked on a development team to successfully commercialize a new optical coating for large-area low emissivity architectural window applications. He graduated with undergraduate degrees in engineering physics and economics from the University of Pittsburgh in 2005 and MS and PhD degrees in materials science and engineering from Carnegie Mellon University in 2006 and 2008, respectively. He has held a position as an adjunct faculty member of the materials science and engineering department at CMU since 2011, is currently the chair of the Energy Conversion and Storage Committee of TMS, and was recently appointed as an associate editor for the Journal of Electronic Materials. He is an author or co-author on approximately 60 technical publications and has submitted more than 12 patent applications with 4 patents successfully issued to date.

Chih-Hung Chang is currently a Professor at the School of Chemical, Biological and Environmental, OSU. He established Oregon Process Innovation Center for sustainable solar cell manufacturing, an Oregon BEST signature research facility, and serve as its director. He received his PhD degree in Chemical Engineering from University of Florida, Gainesville Florida in 1999. He is a SHARP Labs of America scholar and a recipient of NSF CAREER award, Intel Faculty Fellowship. He has been serving as the PI or Co-PI for a number energy-related projects. His group has studied solution based thin film deposition processes, nanomaterials, solar cells, thin film transistors, and microreactor. He has more than 90 peer- reviewed journal publications, 10 issued patents, and 3 pending patents in these areas. He is the founder and acting Chief Science Officer of an OSU-spin out venture, CSD Nano, Inc.

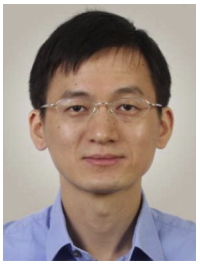

Alan X. Wang is an Assistant Professor of the School of Electrical Engineering and Computer Science at Oregon State University since 2011. He received his Ph.D. degree in Electrical and Computer Engineering from the University of Texas at Austin in 2006. From 2007–2011, he was with Omega Optics, Inc., where he served as the Chief Research Scientist for 9 SBIR/STTR projects. His research interests include nanophotonic devices for optical interconnects, and optical sensors for chemical and biological detection. His current research activities are sponsored by the National Science Foundation, the National Institutes of Health, Oregon Nanoscience and Microtechnologies Institute, the National Energy Technology Laboratory, and industrial sponsors such as Hewlett-Packard. He has more than 50 journal publications and 50 conference presentations, and also holds three U.S. patents. He is a senior member of IEEE and OSA.